Monitoring surface climate with its emissivity derived from satellite measurements

Daniel K. Zhou*, Allen M. Larar, and Xu Liu

NASA Langley Research Center, Hampton, VA, USA

ABSTRACT

Satellite thermal infrared (IR) spectral emissivity data have been shown to be significant for atmospheric research and monitoring the Earth's environment. Long-term and large-scale observations needed for global monitoring and research can be supplied by satellite-based remote sensing. Presented here is the global surface IR emissivity data retrieved from the last 5 years of Infrared Atmospheric Sounding Interferometer (IASI) measurements observed from the MetOp-A satellite. Monthly mean surface properties (i.e., skin temperature T_s and emissivity spectra ε_ν) with a spatial resolution of 0.5×0.5-degrees latitude-longitude are produced to monitor seasonal and inter-annual variations. We demonstrate that surface ε_ν and T_s retrieved with IASI measurements can be used to assist in monitoring surface weather and surface climate change. Surface ε_ν together with T_s from current and future operational satellites can be utilized as a means of long-term and large-scale monitoring of Earth's surface weather environment and associated changes.

Keywords: Remote sensing, ultraspectral instrument, inversion, land surface emissivity.

1. INTRODUCTION

Earth surface spectral emissivity (ε_ν) is a measure of the relative ability of the surface to emit energy by radiation at the frequency ν. It is the ratio of energy radiated by its surface to energy radiated by a blackbody at the same temperature. The value of Earth surface emissivity depends on the composition of the surface materials and varies from location to location and from time to time. Great effort has been devoted toward obtaining and validating Earth's land surface emissivity in a broad wavelength region. Emissivity in the thermal infrared (IR) and microwave regions is particularly interesting as it is crucial for achieving other highly-accurate retrieved parameters, the assimilation of radiances in numerical weather prediction models, climate modeling/monitoring, and studies of the radiation budget for the Earth system.

Data from satellite remote sensors developed for various environmental sensing applications have been useful for deriving surface thermal IR emissivity. For example, emissivity data have been derived using measurements from the Moderate Resolution Imaging Spectroradiometer (MODIS), the Advanced Spaceborne Thermal Emission and Reflection Radiometer (ASTER), the Spinning Enhanced Visible and Infrared Imager (SEVIRI), the Atmospheric InfraRed Sounder (AIRS), and the Infrared Atmospheric Sounding Interferometer (IASI)[1-6]. Emissivity derived from satellite measurements is an "effective" emissivity of the area where the measurement is taken; it depends on the composition of the surface materials in that area. This effective emissivity has been assumed by a linear combination of pure scene types[7,8]. The vegetation cover and soil moisture of the area can significantly affect the emissivity derived from satellite measurements[9,10]. The IR ε_ν derived from IASI measurements has provided spectral information of the surface materials[6] for investigations carried out and reported herein. The aim of this manuscript is to show global ε_ν climatology from the last 5 years of IASI measurements and initial investigation of its seasonal variation over that period of time. The period of 5 years is long enough to observe its variation and to indicate and/or recommend that ε_ν and its trend can be used in assisting surface weather monitoring and climate studies.

*daniel.k.zhou@nasa.gov, Tel: 757-864-5663

2. EMISSIVITY DATA FROM IASI

The Infrared Atmospheric Sounding Interferometer (IASI) was successfully launched into polar orbit aboard the operational polar orbiting MetOp-A satellite on 19 October 2006; significant scientific accomplishments have been made with IASI measurements[11,12]. IASI is a Michelson interferometer with spectral coverage between 3.6 and 15.5 μm. At nadir, the instrument samples data at intervals of 25 km along a cross track, each sample having a maximum diameter of ~12 km. It possesses a continuous spectral coverage from 645 to 2760 cm^{-1} and a high spectral resolution of 0.25 cm^{-1}; in other words, its unapodized spectral resolving power ($\nu/\delta\nu$) is between 2000 to 4000[13]. This higher spectral resolving power benefits retrieving ε_ν simultaneously with T_s and other atmospheric parameters. An inversion scheme, dealing with cloudy as well as cloud-free radiances observed with ultraspectral IR sounders, has been developed and applied to IASI data to retrieve simultaneously atmospheric thermodynamic and surface or cloud microphysical parameters[14]. The data used in this study are produced with the algorithm described by Zhou et al.[6]. Initial IASI ε_ν evaluations were performed[15,16], providing confidence on the accuracy of the products.

Here the so-called "monthly mean climate" dataset (hereafter denoted as MMC) is defined as the monthly mean of all the years of IASI measurements (i.e., from June 2007 to May 2012), while the "monthly mean" is the monthly mean of a certain year (hereafter denoted as MMY). The data have been integrated into a spatial grid of 0.5×0.5-degrees latitude-longitude. IASI ε_ν is spectrally resolved covering all IASI channels. Figure 1 shows the global distributions of December nighttime MMC T_s and ε_ν at a frequency (ν) of 890 cm^{-1} (later simplified as ε_{890}). IASI derived ε_ν shows a seasonal variation, explained by a combination of surface materials, modified from time to time[6]. In other words, the soil moisture, snow/ice cover, and vegetation canopy varies over a different surface backgrounds (e.g., bare soil, sand, and rock mixed surface). Moreover, the ε_ν contains its surface material information in different spectral frequencies, identified in both laboratory and satellite measurements. For instance, emissivity in the quartz reststrahlen bands (750-1250 cm^{-1}) is apparently dominated by the residual mineral quartz[17,18]. Figure 2 illustrates a few ε_ν representing Earth surface materials, which are groups of some similar materials measured in the laboratory[17]. For example, ice ε_ν is smaller than that of water in IR region. Although sea ice ε_ν can vary depending on sea ice type, the ε_ν difference between sea ice and seawater is small but significant, especially in the shortwave region. For instance, using the MMC data of December, the ε_{2400} is 0.981 and T_s is 296.76° K at a location of 0.0-0.5° N Latitude and 149.5-150.0° W Longitude (over seawater); while the ε_{2400} is 0.955 and T_s is 266.74° K at a different location of 59.5-60.0° S Latitude and 149.5-150.0° W Longitude (most likely over sea ice). This helps us to understand why the ε_ν shown in Figure 1b is slightly smaller in the higher latitude regions over the water where sea ice is present.

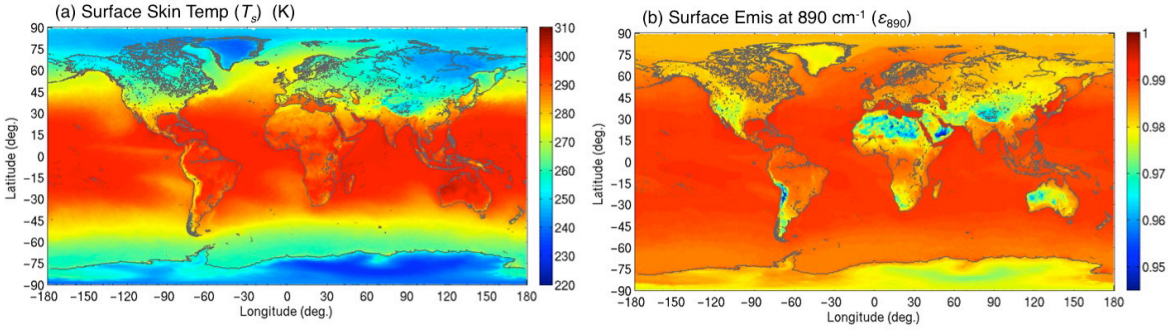

Figure 1. IASI monthly mean climatology: December nighttime (a) surface skin temperature (T_s) and (b) emissivity at 890 cm^{-1} (ε_{890}).

3. EMISSIVITY SEASONAL VARIATIONS AND MONITORING

Because the nature of emissivity does not change rapidly, monthly mean emissivity is used and presented for analysis and monitoring. Emissivity seasonal variation has been indicated in the satellite measurements. For illustration, Figure

3a plots the MMC ε_v measured from Utah over the Rocky Mountains (40.0-40.5° N Latitude; 109.5-110.0° W Longitude; ~1.8 km elevation). Channel emissivity ε_{1100} and ε_{2400} at 1100 cm^{-1} and 2400 cm^{-1}, respectively, for each month is plotted in Figure 3b, showing that the higher emissivity appears in February and July while the lowest one is in April. Surface T_s is plotted in Figure 3c. It implies that snow/ice covers the surface and mostly melts down by April when the emissivity reaches the lowest point with its associated T_s of 276.64° K and fresh-vegetation cover is still at a minimum in the early spring. It increases from April to July when soil moisture might be high and fresh-vegetation cover increases. It then decreases from August to November as vegetation cover decreases.

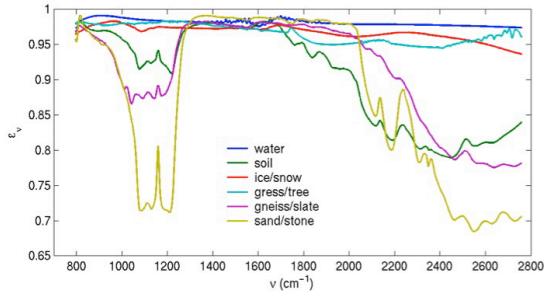

Figure 2. Samples of emissivity spectra representing Earth surface materials.

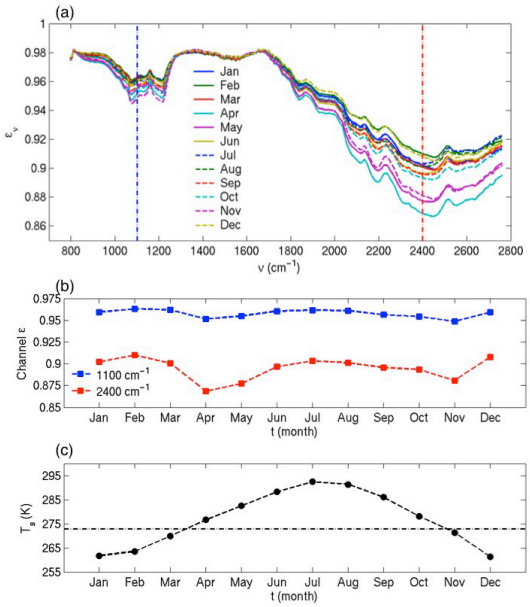

Figure 3. (a) Monthly mean ε_v climatology measured from 40.0-40.5° N Latitude and 109.5-110.0° W Longitude. (b) Channel emissivity at 1100 and 2400 cm^{-1} as a function of time. (c) Surface skin temperature as a function of time.

Although both winter (February) and summer (July) emissivity is relatively high and their difference is small, it is noticed that their spectral shapes are different. For instance, their difference depends on the frequency (or wavenumber). For the case of spring to summer, we assume that flash tree leaves (e.g., Quaking Aspen, common in the area) and some other native vegetation start to grow in the spring. Vegetation cover reaches a maximum by July. We use laboratory-measured white pine tree emissivity, roughly representing a part of the surface materials, and April-measured emissivity to reproduce a combined emissivity to fit July-measured emissivity. Figure 4a shows the combination of 68% of April IASI-measured emissivity and 32% white pine emissivity can closely match July IASI-measured emissivity. Similar analysis has been done for the winter-to-spring case assuming that mixed ice-snow partially covers the ground during the winter season. The April IASI-measured and laboratory-measured ice emissivity are used to make a combined emissivity

to match February IASI-measured emissivity. Figure 4b shows the combination of 54% of April IASI-emissivity and 46% ice emissivity can match February IASI-emissivity. This implies that the emissivity in this region can be used to monitor a relative amount of ice/snow during the winter season.

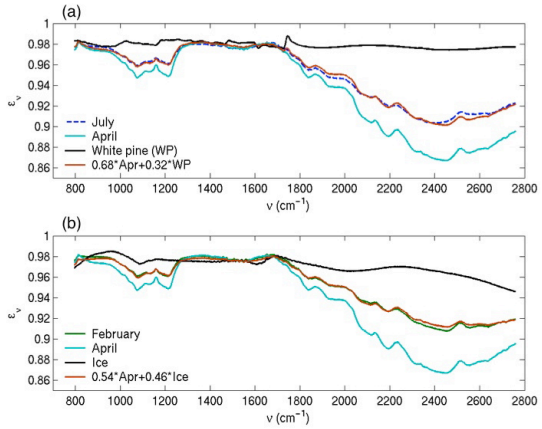

Figure 4. (a) Vegetation increasing from April to July; July ε_ν is roughly reproduced by a linear combination of April ε_ν and white pine ε_ν. (b) Snow/ice covers decreasing from February to April; February ε_ν is roughly reproduced by a linear combination of April ε_ν and ice ε_ν.

We chose IASI channel emissivity at the wavenumber of 975 cm^{-1} (ε_{975}) for a trend analysis and used a few locations to demonstrate that its variation behavior is location dependent. Figure 5 plots monthly mean (a) T_s, (b) T_s anomaly (ϕ_{Ts}), (c) ε_{975}, and (d) ε_{975} anomaly ($\phi_{\varepsilon 975}$) from June 2007 to May 2012. The ϕ_{Ts} (or $\phi_{\varepsilon 975}$) is defined as the monthly mean of the year (MMY) deviated from the monthly mean climatology (MMC). The first location is from the Utah Rocky Mountains as described above. Figure 5c shows the monthly mean ε_{975} (filled red triangle) as a function of time plotted with monthly mean climatology (filled blue circle). The difference (MMY-MMC) or anomaly $\phi_{\varepsilon 975}$ is plotted in Figure 5d. It is clearly evident that "snow/ice" cover varies; for example, January to March 2012 had higher T_s and lower ε_{975} (less snow/ice) than those in the same months during previous years. More snowfall during winter of 2010-2011 led to extra soil moisture and native vegetation during the following 2011 spring and summer. In the figure, the standard deviation errors (shown with error bars) are estimated from a single field-of-view (SFOV) retrieval[6] and then divided by the square root of the number of SFOV retrievals used for a monthly mean in the spatial grid of 0.5×0.5-degrees latitude-longitude. The absolute deviation (i.e., bias) is assumed to be similar in both MMC and MMY data; therefore, the biases roughly cancel each other in their differences (i.e., anomaly ϕ). The red line plots a linear fit of the anomalies, indicating the anomaly trend during this period. At this point, this trend may not be useful in drawing any tendency conclusions, but it certainly can be used for monitoring its variations as more data will be added on from upcoming measurements.

It is worth pointing out that ε_ν variation may not be observed (i.e., no variation) in some places. For example, the monthly mean ε_ν over water is not changed until the water is cold enough to form ice. In Figure 6, the left column is from the equatorial Pacific (0.0-0.5° N Latitude; 139.5-140.0° W Longitude); Figures 6a1 and 6b1 show that T_s is almost seasonally independent except during the period when La Niña and El Niño are currently evident. The ϕ_{Ts} changed from warm to cool between April to May 2010 (Figure 6b1), implying that the tropical Pacific switched from El Niño to La Niña. This was also tracked and confirmed by the NASA/European Ocean Surface Topography Mission/Jason-2 oceanography satellite. As El Niño plays a significant role in tropical drought occurrence[19], a sample from Australia is chosen (right-column of Figure 6: 24.5-25.0° S Latitude; 145.0-145.5° E Longitude) to illustrate ε_ν variation associated with droughts during El Niño years and greater rainfalls during La Niña events. Figures 6c2 and 6d2 plot ε_{975} and $\phi_{\varepsilon 975}$, respectively. The ε increases when soil moisture increases as greater rainfalls occurred; in contrast, the ε decreases when soil moisture decreases as droughts occurred[10,19].

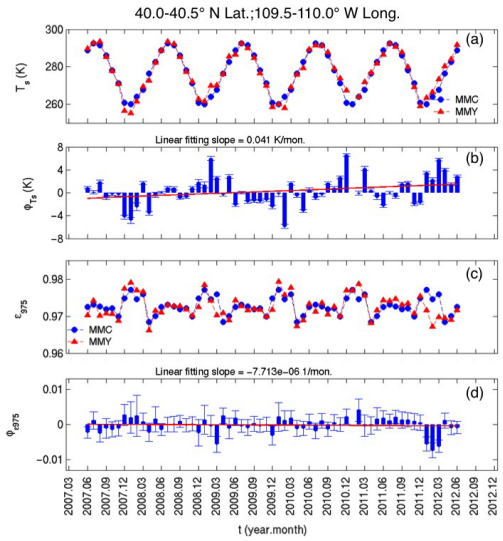

Figure 5. Sample from 40.0-40.5° N Latitude and 109.5-110.0° W Longitude: Illustration of monthly mean (filled red triangle) (a) T_s and (c) ε_{975} against their monthly mean climatology (filled blue circle); and (b) T_s anomalies and (d) ε_{975} anomalies plotted to observe their trends (see text).

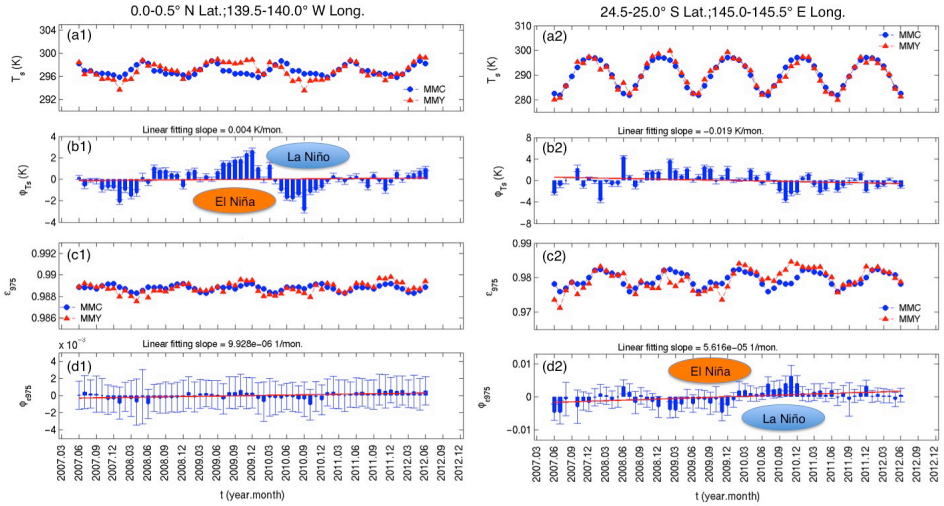

Figure 6. Same as Figure 5 but at 2 other locations: The El Niño (or La Niña) phenomena shown in (b1) causes the land emissivity change shown in (d2) related to the soil moisture, associated with droughts (or great rainfalls).

4. CONCLUSION

We have developed a global climatology atlas of IR ε_s and T_s based on the last 5-years of IASI measurements. The IR ε_s retrieved with IASI measurement is sensitive to surface material. Different surface material is not only reflected in an absolute channel-emissivity value at a certain frequency but also in its spectral shape. Retrieved ε_s shows a temporal variation as its surface and/or surface weather changes. Relatively speaking, the change of surface cover (e.g., vegetation, snow/ice) and soil moisture can be detected with its ε_s depending on the surface background. Month-to-month ε_s variation is clearly evident and it can be significant in some areas such as deserts and bare land. Temporal variation indicates a seasonal diversity; El Niño and/or La Niña effects are evident not only on the water (i.e., equatorial Pacific

T_s), but also on the land surface (i.e., Australia land ε). The different ε for sea ice and seawater might be used, in conjunction with its associated T_s, to monitor the change of global sea ice amounts. Initial findings of emissivity seasonal and inter-annual variation phenomenon at a few locations are reported herein. As the retrieval algorithm continues to be improved to provide higher-quality retrieval data, more investigation and studies with the data during a longer time period are strongly desired to draw explicit conclusions. However, a long-term monitoring of the Earth's surface environment can be critical in assisting weather and climate research. Satellite-measured surface emissivity can be used as a means of long-term and large-scale monitoring of the Earth's environment for climate studies.

ACKNOWLEDGEMENTS

This research is supported by NASA Langley Research Center and NASA Headquarters. The authors wish to specifically acknowledge support from NASA Headquarters Research Division Director Dr. Jack Kaye. IASI was developed and built under the responsibility of the Centre National d'Etudes Spatiales (CNES). It is flown aboard the MetOp-A satellite as part of the EUMETSAT Polar System. The IASI L1C data are received through the Unified Meteorological Archival and Retrieval Facility (UMARF) of EUMETSAT.

REFERENCES

[1] Z. M. Wan, and Z. L. Li, "A physics-based algorithm for retrieving land-surface emissivity and temperature from EOS/MODIS data," IEEE Trans. Geosci. Remote Sens., **35**, 980-996 (1997).

[2] G. C. Hulley, S. J. Hook, and A. M. Baldridge, "ASTER land surface emissivity database of California and Nevada," Geophys. Res. Lett., **35**, L13401 (2008).

[3] I. F. Trigo, L. F. Peres, C. C. DaCamara, and S. C. Freitas, "Thermal land surface emissivity retrieved from SEVIRI/Meteosat," IEEE Trans. Geosci. Remote Sens., **46**, 307-315 (2008).

[4] E. A. Péquignot, Chédin, and N. A. Scott, "Infrared Continental Surface Emissivity Spectra Retrieved from AIRS Hyperspectral Sensor," J. Appl. Meteorol. Climatol., **47**, 1619-1633 (2008).

[5] J. Li, J. Li, E. Weisz, and D. K. Zhou, "Physical retrieval of surface emissivity spectrum from hyperspectral infrared radiances," Geophys. Res. Lett., **34**, L16812 (2007).

[6] D. K. Zhou, A. M. Larar, X. Liu, W. L. Smith, L. L. Strow, P. Yang, P. Schlüssel, and X. Calbet, "Global land surface emissivity retrieved from satellite ultraspectral IR measurements," IEEE Trans. Geosci. Remote Sens., **49**, 1277-1290 (2011).

[7] R. O. Knuteson, F. A. Best, D. H. DeSlover, B. J. Osborne, H. E. Revercomb, W. L. Smith, Sr., "Infrared land surface remote sensing using high spectral resolution aircraft observations," Advances In Space Research, **33**, 1114-1119 (2003).

[8] G. C. Hulley, S. J. Hook, E. Manning, S.-Y. Lee, and E. Fetzer, "Validation of the Atmospheric Infrared Sounder (AIRS) version 5 land surface emissivity product over Namib and Kalahari deserts," J. Geophys. Res., **114**, 9104.1–9104.11 (2009).

[9] S. Ringrose, W. Matheson, P. Wolski, and P. Huntsman-Mapila, "Vegetation cover trends along the Botswana Kalahari transect," Journal of Arid Environments, **54**, 297-317 (2003).

[10] M. Mira, E. Valor, V. Caselles, E. Rubio, C. Coll, J. M. Galve, R. Niclòs, J. M. Sánchez, and R. Boluda, "Soil moisture effect on thermal infrared (8–13 μm) emissivity," IEEE Trans. Geosci. Remote Sens., **48**, 2251-2260 (2010).

[11] G. Chalon, F. Cayla, and D. Diebel, "IASI: An Advanced Sounder for Operational Meteorology," Proceedings of the 52nd Congress of IAF, Toulouse, France, 1-5 (2001).

[12] F. Hilton, and co-authors, "Hyperspectral Earth Observation from IASI: four years of accomplishments," Bull. Amer. Meteor. Soc., **93**, 347–370 (2012).

[13] W. L. Smith, Sr., H. Revercomb, G. Bingham, A. Larar, H. Huang, D. Zhou, J. Li, X. Liu, and S. Kireev, "Technical Note: Evolution, current capabilities, and future advances in satellite ultra-spectral IR sounding," Atmos. Chem. Phys., **9**, 5563-5574 (2009).

[14] D. K. Zhou, W. L. Smith, A. M. Larar, X. Liu, J. P. Taylor, P. Schlüssel, L. L. Strow, and S. A. Mango, "All weather IASI single field-of-view retrievals: case study - validation with JAIVEx data," Atmos. Chem. Phys., **9**, 2241-2255 (2009).

[15] Z. Li, J. Li, X. Jin, T. J. Schmit, E. E. Borbas, and M. D. Goldberg, "An objective methodology for infrared land surface emissivity evaluation," J. Geophys. Res., **115**, D22308 (2010).

[16] Z. Yao, J. Li, J. Li, and H. Zhang, "Surface emissivity impact on using hyperspectral infrared sounder data over land," J. of Appl. Meteor., **50**, 1225-1235 (2011).
[17] J. W. Salisbury, and D. M. D'Aria, "Emissivity of terrestrial material in the 8-14 μm atmospheric window," Remote Sens. Environ., **42**, 83-106 (1992).
[18] G. C. Hulley, S. J. Hook, E. Manning, S.-Y. Lee, and E. Fetzer, "Validation of the Atmospheric Infrared Sounder (AIRS) version 5 land surface emissivity product over Namib and Kalahari deserts," J. Geophys. Res., **114**, 9104.1–9104.11 (2009).
[19] C. A. S. Coelho, and L. Goddard, "El Niño-induced tropical droughts in climate change projections," J Climate, **22**, 6456–6476 (2009).